




Cite this: DOI: 10.1039/c9nr09251j

Nanoparticle translocation across the lung surfactant film regulated by grafting polymers[†]

Xuan Bai,^{‡a,b,c} Mujun Li^{‡b,c} and Guoqing Hu^{‡a*} 

Nanoparticle-based pulmonary drug delivery has gained significant attention due to its ease of administration, increased bioavailability, and reduced side effects caused by a high systemic dosage. After being delivered into the deep lung, the inhaled nanoparticles first interact with the lung surfactant lining layer composed of phospholipids and surfactant proteins and then potentially cause the dysfunction of the lung surfactant. Conditioning the surface properties of nanoparticles with grafting polymers to avoid these side effects is of crucial importance to the efficiency and safety of pulmonary drug delivery. Herein, we perform coarse-grained molecular simulations to decipher the involved mechanism responsible for the translocation of the polymer-grafted Au nanoparticles across the lung surfactant film. The simulations illustrate that conditioning of the grafting polymers, including their length, terminal charge, and grafting density, can result in different translocation processes. Based on the energy analysis, we find that these discrepancies in translocation stem from the affinity of the nanoparticles with the lipid tails and heads and their contact with the proteins, which can be tuned by the surface polarity and surface charge of the nanoparticles. We further demonstrate that the interaction between the nanoparticles and the lung surfactant is related to the depletion of the lipids and proteins during translocation, which affects the surface tension of the surfactant film. The change in the surface tension in turn affects the nanoparticle translocation and the collapse of the surfactant film. These results can help understand the adverse effects of the nanoparticles on the lung surfactant film and provide guidance to the design of inhaled nanomedicines for improved permeability and targeting.

Received 30th October 2019,
Accepted 22nd January 2020

DOI: 10.1039/c9nr09251j

rsc.li/nanoscale

Introduction

Design of nanoparticles (NPs) as carriers for drug delivery to the human body has attracted more and more attention due to their diverse applications in nanomedicines.^{1,2} As a major route for systemic drug delivery, the lung is advantageous over other entries, such as oral delivery or injection, due to its high permeability, large surface area for rapid adsorption, and non-invasion.^{3,4} However, NP delivery to the lung still faces the challenge mainly caused by the air–blood barrier that hinders the entry of NPs into the body circulation.^{5,6}

A lung surfactant is a lipid–protein mixture which is composed of 85% phospholipids, 5% cholesterol and ~10% surfactant proteins (SP-A, B, C and D) and is synthesized by the type

II alveolar epithelial cells.⁷ Due to its amphipathicity, the lung surfactant adsorbs onto the surface of the alveoli and forms a monolayer or multilayer film covering the entire surface, which can reduce the surface tension to maintain the normal tidal respiration.^{7–9} Among the surfactant proteins, SP-B and SP-C are small hydrophobic proteins that play a crucial role in regulating the biophysical function of the lung surfactant.¹⁰ SP-A and SP-D are weakly associated with the surfactant film and play an important role in lung host defense.¹¹

When NPs deposit into the deep lung, they inevitably interact with this film first. Whether the NPs are permeable through this barrier depends on the physicochemical properties of NPs and the biophysical properties of the film.^{12–15} The interactions between the NPs and the surfactant film also potentially cause the dysfunction of the lung surfactant if the NPs are embedded in the film or deplete the lipids or proteins of the film.^{16–19} Meanwhile, the adsorbed lipids and proteins on the NPs will modify the surfaces of the NPs and cause profound effects on the subsequent bio-interactions of the NPs, for example, influencing the clearance by alveolar macrophages and the uptake of alveolar epithelial cells.^{20–24}

Surface modification of NPs can improve their bio-compatibility or functionality.^{25,26} It is efficient to eliminate the unde-

^aDepartment of Engineering Mechanics, Zhejiang University, Hangzhou 310027, China. E-mail: ghu@zju.edu.cn

^bThe State Key Laboratory of Nonlinear Mechanics (LNM), Institute of Mechanics, Chinese Academy of Sciences, Beijing 100190, China

^cSchool of Engineering Science, University of Chinese Academy of Sciences, Beijing 100049, China

[†]Electronic supplementary information (ESI) available. See DOI: 10.1039/c9nr09251j

[‡]These authors contributed equally to this work.

sirable adsorption of proteins on the long blood circulation or to enhance the drug delivery to the lung by coating the surface of NPs with polymers, such as polyethylene glycol (PEG).^{27–30} One of the central questions regarding the pulmonary NP delivery to the lungs is how to design and control the material properties to achieve a high permeation through the lung surfactant film with minimized toxicity. Biophysical studies have pinpointed the importance of such polymeric coatings in the lung surfactant inhibition by deposition of NPs, where the inhibition level of the lung surfactant depends on the type of grafting polymer and the surface charge.^{31–33} However, in these *in vitro* studies, the NPs were injected into the lung surfactant film from the liquid phase, different from the natural translocation process of the aerosol or airborne NPs originating from the air phase. Moreover, the mechanism of such translocation behavior can be hardly provided without a detailed assessment of the roles of the physicochemical properties of the grafting polymers. The coarse-grained molecular dynamics (CGMD) simulations, which have been widely used for studying the interactions between the NPs and the biomembranes, help understand the mechanism responsible for NP translocation at the molecular level.^{12,34–37} To the best of our knowledge, the interactions between the polymer grafting NPs and the lung surfactant films have not yet been investigated *via* molecular dynamics simulations.

In this paper, we performed CGMD simulations to explore the roles of the physicochemical properties of the grafting polymers in the translocation process, based on a PEGylated NP–lung surfactant monolayer model system. First, we found that the Au NPs grafted with different types of polymers experienced distinct translocation processes. Next, we demonstrated that these differences stem from their interaction strength with either the hydrophobic or the hydrophilic components of the film, which is correspondingly related to their surface polarity and surface charge. The hydrophobic proteins can promote the penetration by adsorbing onto the surface of the NPs. Finally, we examined the interplays between the NP translocation and the biophysical properties of the lung surfactant film.

Model and methods

System setup

The system setup included a water slab with two symmetric monolayers at the air–water interfaces and two NPs initially deposited above and below the center of the monolayer of 12 nm, respectively, which was centered at a simulation box (30 nm × 30 nm × 100 nm) (Fig. 1). The water slab was large enough to avoid the interaction between the two monolayers. This symmetric arrangement allows us to conveniently set up the system boundaries without compromising the accuracy of simulating monolayers or significantly increasing the computational load. The monolayer was constructed using the PACKMOL package.³⁸ Consistent with our previous simulations, each monolayer contained three types of lipids: 1120 dipalmitoylphosphatidylcholine (DPPC) molecules, 480 palmi-

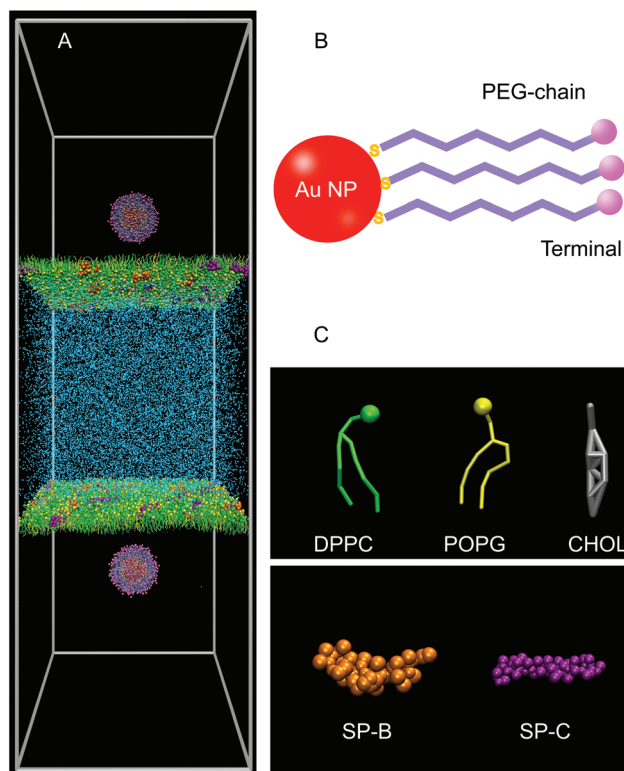


Fig. 1 (A) Initial setup of the MD simulation system. The simulated symmetric system consists of a water slab sandwiched between two surfactant monolayers and two NPs initially placed at the air phase. (B) The illustration of the NP–PEG complex used in the simulation. The atoms at the NP surface are grafted with the PEG chains *via* sulfur. The terminals of the PEG chains are functionalized with amino or carboxyl to feature the different surface charges. (C) The CG structure of the individual components of the lung surfactant in our simulations.

toyl-oleoylphosphatidylglycerol (POPG) molecules and 112 cholesterol molecules, doped with two types of hydrophobic surfactant proteins, mini-B and SP-C.^{12,20} DPPC is a zwitterionic lipid with a net charge of 0. POPG is an anionic lipid with a net charge of -1 . Our lung surfactant model consists of 62% PC (DPPC), 26% PG and unsaturated phospholipid (POPG), 6% cholesterol and 6% surfactant protein (SP-B + SP-C) in weight. This lung surfactant model is analogous to the real lung surfactant, which consists of 69% PC (36% DPPC and 33% unsaturated PC), 10% anionic phospholipid (PG), 5–10% cholesterol and 10% protein (2% SP-B + SP-C) in weight.⁷ Note that we did not include SP-A and SP-D here. The monolayer was well equilibrated at different constant surface tensions of 10, 20, and 40 mN m⁻¹ before interacting with the NPs. No external force was applied on the NPs during the simulations. Each NP consisted of a core of a bare gold NP with a radius of about 3.2 nm and a shell formed by grafted PEG chains. The terminals of the grafted chains of some NPs were functionalized with two typical groups: amino or carboxyl, to feature the different surface properties of the functionalized polymeric NPs.³⁹ Na⁺ ions or Cl⁻ ions were added into the water slab to neutralize the system.

Simulation details

The standard MARTINI force field was adopted in our simulations.⁴⁰ In the CGMD simulation, a group of atoms is considered to be one bead to extend the time and space scale of the simulation along with maintaining their physicochemical properties, such as charge and polarity, which can capture the features of the NP–monolayer interactions. The structure and topology of the protein were derived from the all-atom models downloaded from the protein data bank⁴¹ (PDB ID: 2DWF for mini-B and 1SPF for SP-C) using the martinzi.py script. Here, mini-B (PDB ID: 2DWF) is a 34-residue peptide composed of the N- and C-terminal helical regions of the full-length 79-residue SP-B, which has been proved to capture certain activity of the full-length SP-B.⁴² Two tails of the SP-C peptide (PDB ID: 1SPF) have been palmitoylated, which is crucial for its surface activity.⁴³ The net charge of the modeled SP-B is +4 and that of the modeled SP-C is +3 in our simulations, which are comparable to the SP-B and SP-C with a net charge of +7 and +3 respectively in the natural human lung surfactant.⁴⁴ The Au NPs were constructed with the bead type C5, with each Au atom represented by one CG bead. The PEG monomers were represented by bead type SN0, with the terminals being represented by SP2 for the neutral terminal, Q_a for the anionic terminal and Q_d for the cationic terminal. The standard MARTINI water model was adopted with no partial charges.

During the simulations, the NPT ensemble was used to equilibrate the lung surfactant monolayer and simulate the NP–monolayer interactions under a constant surface tension. The NVT ensemble was used to simulate the NP–monolayer interactions at a constant surface area. NPs, lipids, water, and proteins were coupled separately to a temperature of 310 K by *v*-rescale temperature coupling with a time constant of 1 ps. The pressure boundary conditions were set using the semi-isotropic Berendsen pressure coupling method with a coupling constant of 4 ps. The system compressibility was set to $5 \times 10^{-5} \text{ bar}^{-1}$ in the *x*–*y* direction and 0 in the *z*-direction to maintain the box length along the *z* axis constant. The standard cutoffs for the MARTINI force field were used for non-bonded interactions: the Lennard-Jones (LJ) potential was shifted to zero between 0.9 and 1.2 nm to approximate the non-electrostatic interactions, and the Coulomb potential was shifted to zero between 0 and 1.2 nm with a global relative dielectric constant of 15 to calculate the electrostatic interactions. The time step was 10 fs with the neighbor list updated every 10 steps. Each simulation was performed for 200 ns to reach equilibrium. The simulations performed under pertinent conditions are summarized in Table S1 in the ESI.† All simulations were performed using the Gromacs 5.2.2.⁴⁵

Results and discussion

Translocation of polymeric NPs depends on the properties of the grafting polymers

When a NP docks on a bio-membrane, it will initiate various physicochemical interactions that are governed by their

electrostatic, van der Waals, hydrophobic forces and so on.^{46–49} These forces are associated with the physicochemical properties of the NPs and the biophysical properties of the membrane. By regulating the varied grafting conditions, such as monomer number per chain, grafting density, and terminal charge, we can control some basic properties of the polymeric NPs, including the surface charge density, surface polarity, and the diameter. Considering the equilibrium surface tension of the adsorbed lung surfactant film to be about 20 mN m^{-1} ,^{7,50} we first simulated the translocation processes of these NPs across a static lung surfactant monolayer with a surface tension of about 20 mN m^{-1} by initially depositing the NPs at the air phase (the initial setup is shown in Fig. 1A). We found that the translocations of the NPs can be generally classified into four types: retention at lipid tails, adhesion onto lipid heads, penetration with the adsorption of lipids or proteins, and penetration without adsorption (Fig. 2).

Among these, all the neutral NPs can spontaneously penetrate the monolayer, while the charged NPs grafted with short polymers (5 monomers) with a high grafting density (100%) are blocked by the hydrophobic surface of the monolayer, leading to a retention at the lipid tails. As the length of the grafting polymer increases to 10 monomers or the grafting density decreases to 60% or 20%, the charged NPs can penetrate this hydrophobic barrier to reach the water phase, possibly due to the decrease in their surface charge density. To eliminate the randomness of simulations, we repeated the simulation of the translocation of the negatively charged NPs (grafted with chains of 5 or 10 monomers with a grafting density of 100%) 3 times. We found that the randomness of the simulations does not affect the penetration of the NPs. We further investigated the translocation of the negatively charged NPs (grafted with chains of 7 and 8 monomers with a grafting density of 100%) to study the effect of the length of the grafting polymers (as shown in Fig. S1†). It is found that the increase in the length of the polymer can promote the penetration of the charged NPs.

When the NPs come to the hydrophilic surface of the monolayer, most of the positively charged NPs will adhere to the monolayer and lead to the local bending of the monolayer (especially in cases of the NPs grafted with chains of 5 monomers with a grafting density of 60% and the NPs grafted with chains of 10 monomers with a grafting density of 100%), which probably results from their strong electrostatic interactions with the anionic lipids. In contrast, after the negatively charged and neutral polymeric NPs penetrate the monolayer, no obvious adhesion is observed. In some cases, the negatively charged and neutral NPs will attract lipids or proteins to their surfaces, which potentially causes certain adverse effects on the lung surfactant. The similar protein depletion behavior of the negatively charged NPs was observed in our previous simulations.¹² In other cases, the negatively charged and neutral NPs can completely penetrate the monolayer without disturbing the monolayer structure. Collectively, the tunable polymeric coatings can significantly influence the translocation of

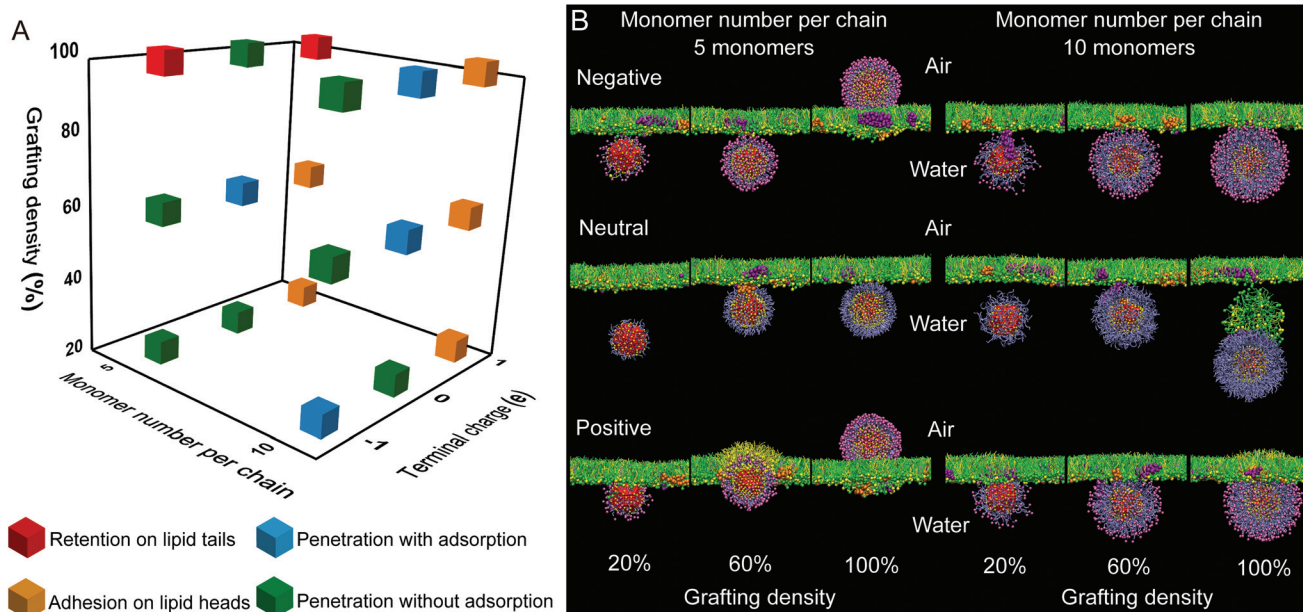


Fig. 2 Final states (A) and the corresponding snapshots (B) of the NPs under different grafting conditions after interacting with the lung surfactant film. The final states are defined as the final positions of the NPs and the adsorption of the lipids or proteins onto the NP surface. The grafting density is defined as the ratio of the amount of the surface Au atoms that were grafted with polymers to the total amount of the surface Au atoms.

the NPs through the lung surfactant monolayer by conditioning the physicochemical properties of the NPs.

Effect of the interactions between the NPs and the different lung surfactant components on translocation

Given that the penetration of NPs can be hindered by either the hydrophobic part or the hydrophilic part of the monolayer, we suppose that the translocation of the NPs is controlled by their affinity with the tails and the heads of the phospholipids. Herein, we analyze their interaction energies to confirm this hypothesis. We begin the analysis by comparing the negatively charged NPs grafted with chains of 5 monomers with grafting densities of 20% and 100% (one of them stays at the tails and the other one totally penetrates the monolayer). It is found that the NPs grafted with fewer polymers can readily penetrate the film (Fig. 3A) due to their smaller size or higher van der Waals (VDW) interaction energy with the lipid tails (Fig. 3B) that may be provided by the exposed neutral PEG beads. To eliminate the size effect, we replace the terminal charge beads of the larger NPs with the neutral PEG beads to meet an equal surface charge density (1.07 e nm^{-2}) to that of the smaller NPs. As a result, the reduction in the surface charge enables a stronger interaction with the lipid tails for the NPs, thus allowing the penetration across the monolayer (Fig. 3C). This is because the neutral groups have a lower polarity than the charged ones, therefore interacting with the apolar lipid tails more strongly. Similarly, the NPs can more readily penetrate the monolayer when their surface polarity decreases with the increase in the grafted-polymer length (Fig. 2). Thus, we deduce that moderate surface polarity can enhance the adhesion between the NPs and the lipid tails to promote the

tails to wrap the NPs, whereas high surface polarity will hinder the active penetration.

We further studied the effect of the interactions between the NPs and the lipid heads on the translocation process by comparing the two different charged NPs (Fig. 4). Fig. 4A and B show that the positively charged NPs take a longer time to penetrate the film than the negatively charged ones, and also adhere to the film after penetration. Interestingly, from the energy interaction diagram, we find that the adhesion of the positively charged NPs not only results from their stronger electrostatic interaction with the anionic lipids of the film but also from their stronger VDW interactions (Fig. 4B). We then examined the amount of the head beads of the adsorbed lipid around the surfaces of these two charged NPs. Fig. 4C clearly shows that the positively charged NPs cluster the lipids around their surface during the penetration, while the negatively charged ones repulse the lipids. Therefore, the positively charged NPs will suffer larger attractive forces from the lipid heads, which delay the penetration and also result in the adhesion to the film leading to a visible curvature (Fig. 4A). Generally, the surface polarity and surface charge can affect the interactions of the NPs with the lipid tails and heads respectively, thus resulting in distinct translocation processes. Next, we investigated how the surfactant proteins affect the translocation process of NPs.

To study the effect of the surfactant proteins, we removed the proteins from the film for comparison. Surprisingly, under the same surface tension, the translocation of the negatively charged NPs is hindered as the NPs remain at the hydrophobic tails of the film in the absence of the proteins (Fig. 5A). The interaction energy curve shows that the proteins do not influ-

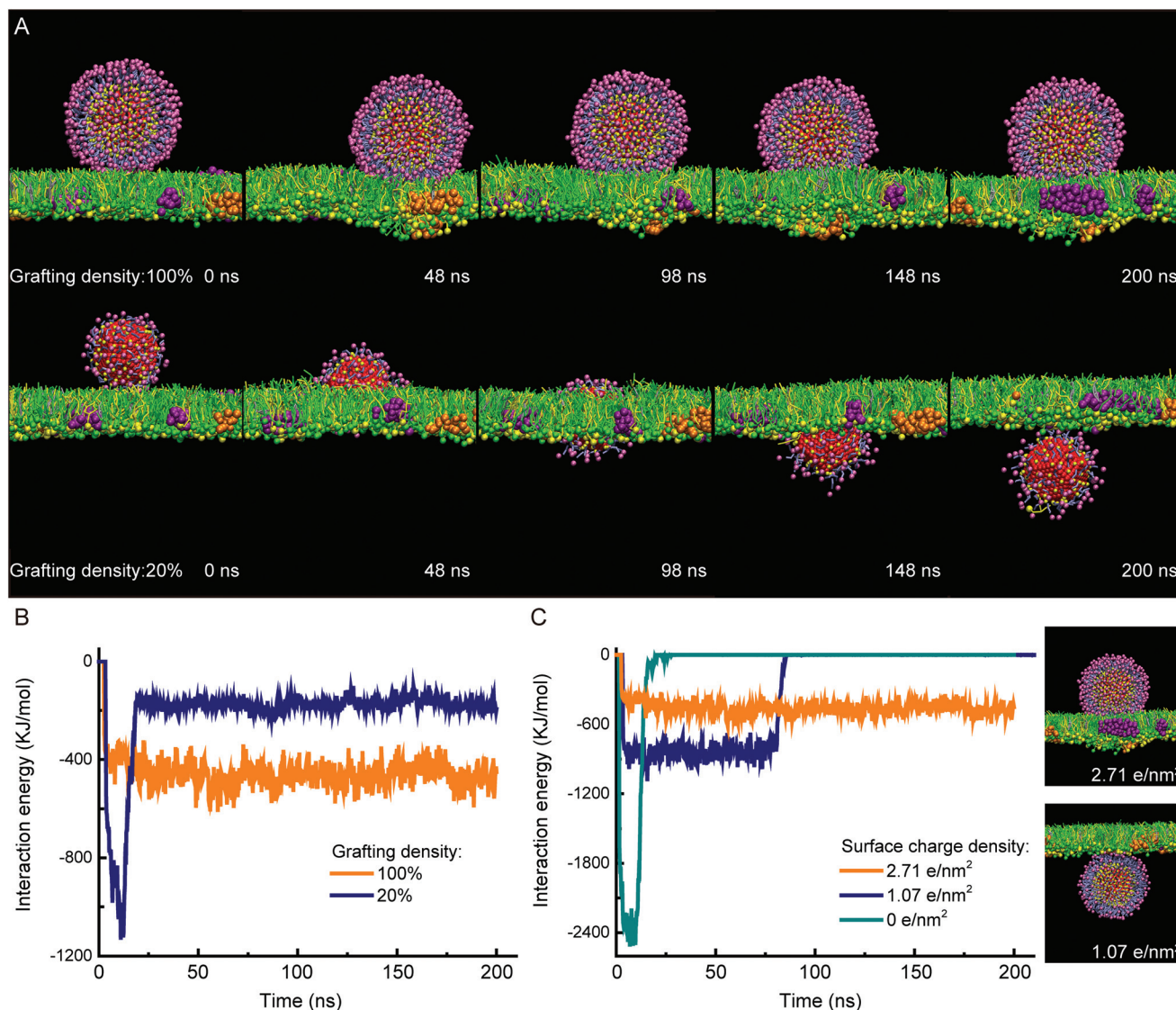


Fig. 3 Effect of the interactions between NPs and lipid tails on the translocation. (A) Visualization for the time sequences of the translocation process of the negatively charged NPs (grafted with chains of 5 monomers with different grafting densities). (B) The interaction energy between the lipid tails and the negatively charged NPs (grafted with chains of 5 monomers with different grafting densities). (C) The interaction energy between the lipid tails and the NPs with different surface charges (grafted with chains of 5 monomers with a grafting density of 100%).

ence the strength of interaction between the NPs and the lipid tails but provide an extra attractive energy when the NPs penetrate the film (Fig. 5A and B). The corresponding snapshots of the protein–NP organization are shown in Fig. 5C, where the hydrophobic SP-C protein is initially inserted at the interface between the lipid heads and tails. When the NPs reach this interface, their passage is accompanied by the repulsion of the surrounding lipids or proteins near the NPs, which can generate a pore on the film to allow the penetration. By interacting with the protein, NPs can haul out the protein from the film to help the pore formation (Fig. 5C). After the penetration, the adsorbed proteins detach from the NP surface and return to the film. It should be noted that in some cases, the adsorbed protein may be pulled out into the liquid phase that detaches

from the film. Note that the energy obtained in our simulations is the interaction energy, which is different from the free energy calculated by applying an external force. Nevertheless, free energy consideration of the translocation of the polymer-grafted NPs across the monolayer, such as the entropic effects and the morphology changes of the grafting polymers during the translocation,^{51–53} needs further investigations.

Our simulations pinpoint the importance of the interactions between the NPs and the multiple components (such as lipid tails, lipid heads, and surfactant proteins) of the lung surfactant in the translocation of the NPs, which can help revise the previous lung surfactant models that only include DPPC or some other phospholipids.^{54–56} However, the natural

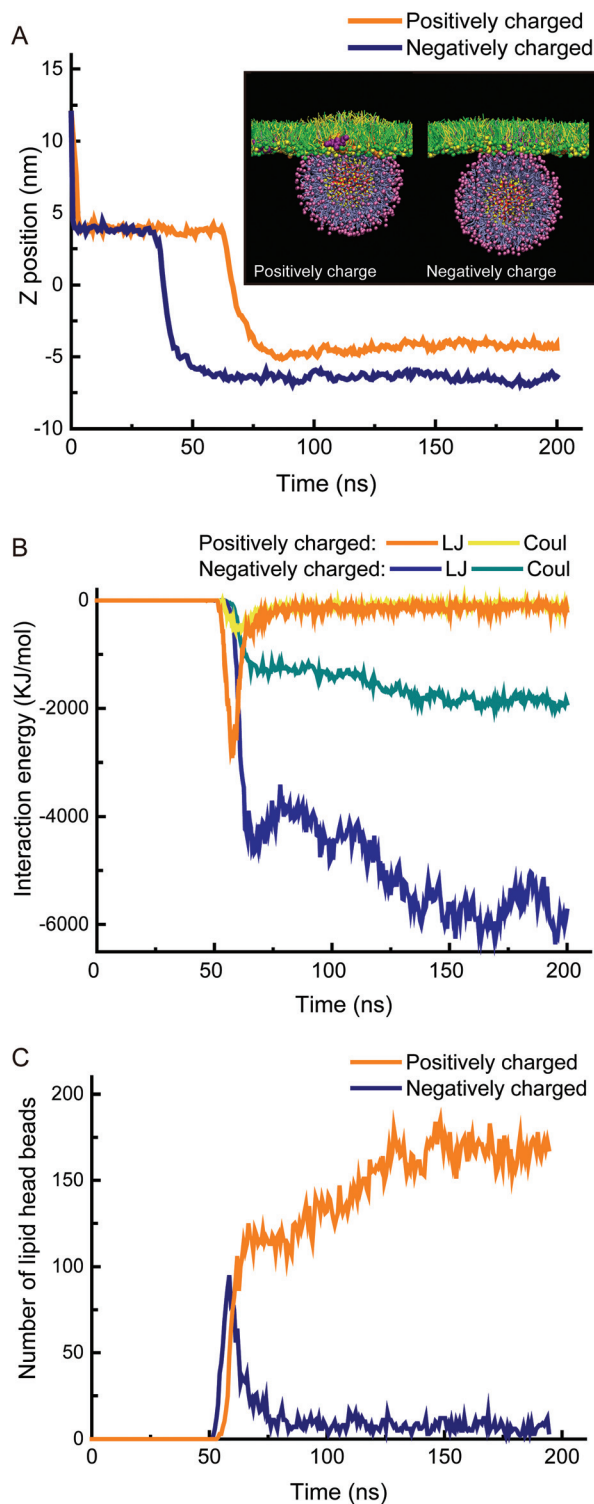


Fig. 4 Effect of the interactions between NPs and lipid heads on the translocation. The NPs are grafted with chains of 10 monomers with a grafting density of 100%. (A) The dynamic Z position of the NPs with different surface charges. The position is defined as the Z distance between the center of the NP and the center of lipids. (B) The interaction energy between the lipid heads and the NPs. LJ stands for van der Waals (VDW) interactions and Coul stands for electrostatic interactions. (C) The number of lipid head beads that attach to the surface of the two NPs. The interaction range is set to 0.47 nm, which is the equilibrium distance between two beads in the MARTINI force field.

human lung surfactant is far more complex than the present model. For example, the natural lung surfactant film is more than a monolayer at the surface of the lung fluids that coexist with underlying multilayers.⁵⁷ Such multilayers may hinder the subsequent translocation of the NPs due to the adhesion of the NPs on the surface of the multilayer. Besides, our simulations do not capture all the properties of the native SP-B because its structure is more complex than that of the mini-B in our simulations. It is necessary to develop a more sophisticated lung surfactant model to study the roles of the different components in the NP–lung surfactant interactions, using a much more powerful computing resource. In general, the present model suggests that moderate surface polarity and charge can promote the NP translocation across the surfactant film. However, how the translocation of these NPs affects the biophysical properties of the lung surfactant monolayer remains unclear, which is addressed in the next section.

Interplays between the NP translocation and the biophysical properties of the lung surfactant film

As mentioned before, the translocation of the NPs may influence the structure and the function of the lung surfactant film, which directly stems from the interactions between the NPs and the surfactant lipids or proteins. Given that the positively charged NPs can adsorb the lipids and the neutral NPs can deplete the lipids during translocation, we first describe the local structure of the adsorbed lipids around the NP surface by comparing their components (represented as the molar ratios) with those of the natural lung surfactant film (Fig. 6A). It is found that the anionic phospholipids are enriched with positively charged NPs as the NPs adhere to the lipid heads, possibly due to their strong electrostatic interactions. The composition of the adsorbed lipids on the neutral NPs is similar to that of the natural film, indicating that such depletion of the lipids is non-selective. Due to the inhomogeneous distribution of the surfactant proteins, we performed another five independent runs by replacing the NPs at different initial positions to study the interactions during the penetration of the negatively charged or neutral NPs. Note that here we do not present the data of the depletion by the positively charged NPs because the simulations show that they have no depletion effect on the lipids or proteins (Fig. 2). The classification of the final states of the above simulations is shown in Fig. 6B and the corresponding snapshots are shown in Fig. S2.† It is found that the negatively charged NPs are more likely to deplete the proteins, particularly the SP-B, by dragging them to the water phase, which is similar to our previous computational observations.¹² Although the neutral NPs are more likely to penetrate the film without depletion, they will possibly drag out the lipids and the SP-C to the water phase, which is hardly observed in the penetration of the negatively charged NPs.

By altering the lipid configuration or depleting the proteins, the penetration of the NPs will consequently affect the surface tension of the film. Fig. 6C shows the variation of the surface

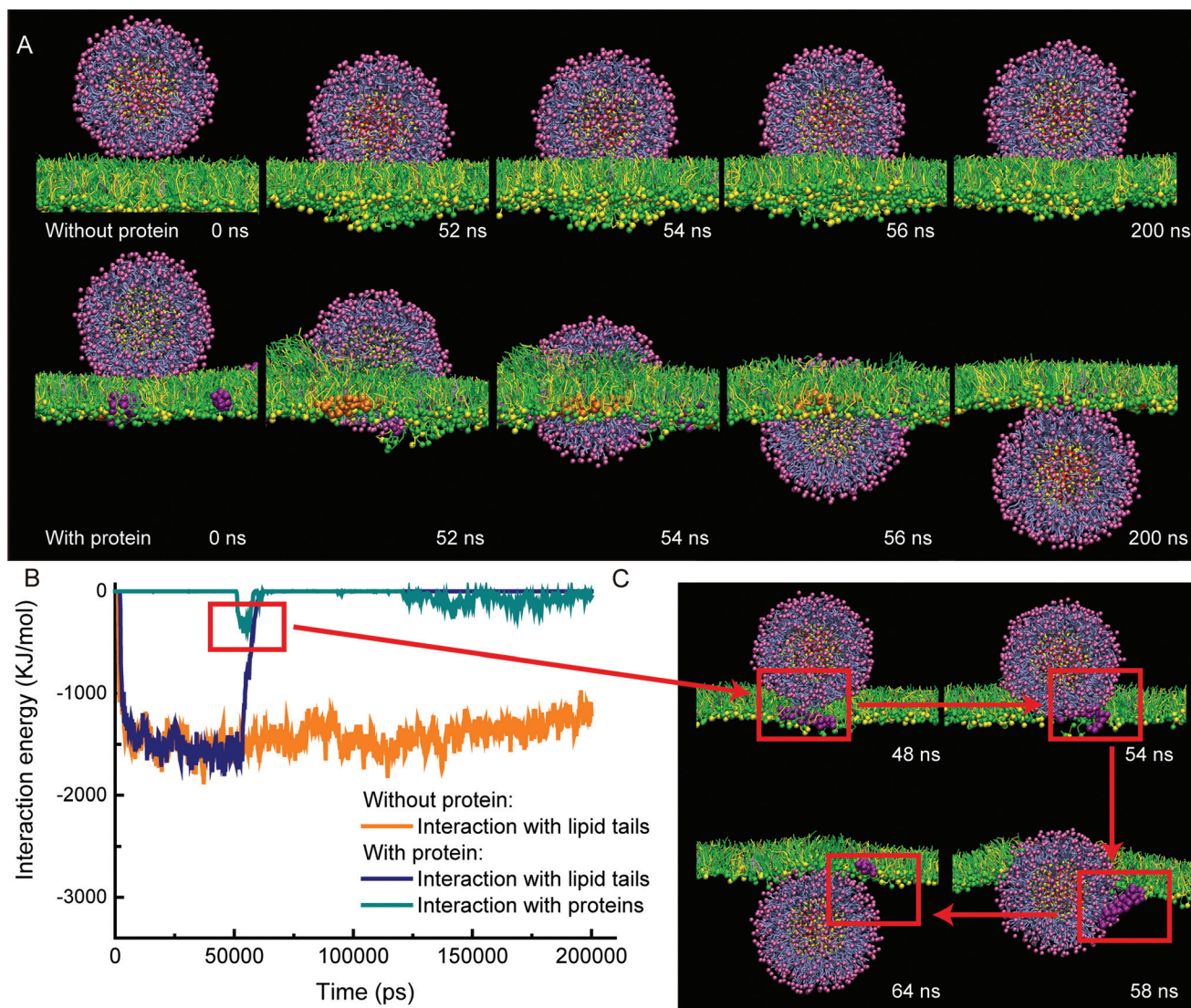


Fig. 5 Effect of the interactions between NPs and proteins on the translocation. The NPs are grafted with chains of 10 monomers with a grafting density of 100% with the negatively charged terminal. (A) The translocation process of the NPs through the lung surfactant film with and without surfactant proteins. (B) The interaction energy between NPs and the lipid tails or surfactant proteins. (C) Illustration of the NP–protein interaction as the NP penetrates the film by generating a pore.

tension of the film after the penetration. The surface tension of the film is not significantly increased by the adhesion of a positively charged NP or the depletion of a surfactant protein by a negatively charged NP. The toxicity of these NPs becomes severe only after more proteins are depleted by many NPs, which agrees with an experimental finding on the dose-dependent toxicity of the inhaled NPs.⁵⁸ Occasional depletion of lipids by a neutral NP can be compensated by the quick adsorption of the bulk lipids from the subphase onto the film.⁵⁹

The biophysical properties of the lung surfactant film will in turn affect the NP penetration due to the change in the lipid packing. During breathing, the lung surfactant film is continuously subjected to expansion–compression cycles, varying the surface tension from tens of mN m^{-1} to near zero. Herein, we

consider the surface tensions of 40 mN m^{-1} and 10 mN m^{-1} to mimic the expansion and compression states of the film. As the surface tension decreases from 40 mN m^{-1} to 10 mN m^{-1} , the lipid chain becomes more ordered and more closely packed, indicating that the lung surfactant film undergoes a phase separation from the liquid expanded–liquid condensed phase to the liquid condensed phase (Fig. S3†).⁶⁰ As expected, the close packing of the lipids (*i.e.*, more lipids in a given area at 10 mN m^{-1}) will delay or hinder the translocation of the negatively charged NPs across the film (Fig. 7A and B). Then, we compare the interaction energies between the lipid tails and the charged/neutral NPs (as shown in Fig. S4†). Under two different surface tensions, the strengths of interactions of the lipid tails with the neutral NPs are both much stronger than those with the negatively charged NPs. Thus, we can deduce

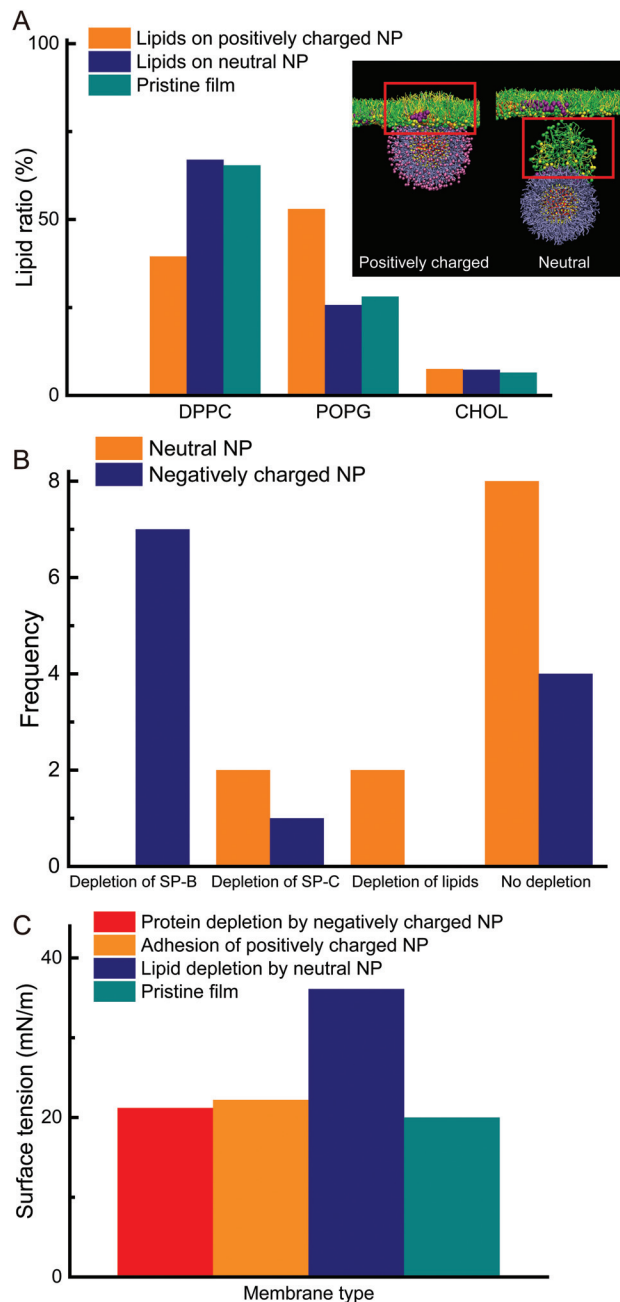


Fig. 6 Influences of the translocation of the NPs on the biophysical properties of the lung surfactant film. (A) Composition of the lipids that attach to the surfaces of the positively charged and neutral NPs. (B) Classification of the equilibrated states of the negatively charged and neutral NPs after interacting with the lung surfactant film. (C) Effect of the translocation of the different NPs on the surface tension of the film.

that the strong interaction energy between the neutral NPs and the lipid tails would result in the agile penetration of the neutral NPs that depends weakly on the surface tension. On the other hand, the surface tension may play a more important role in regulating their translocation because the interaction strengths of the lipid tails with the negatively charged NPs are relatively low.

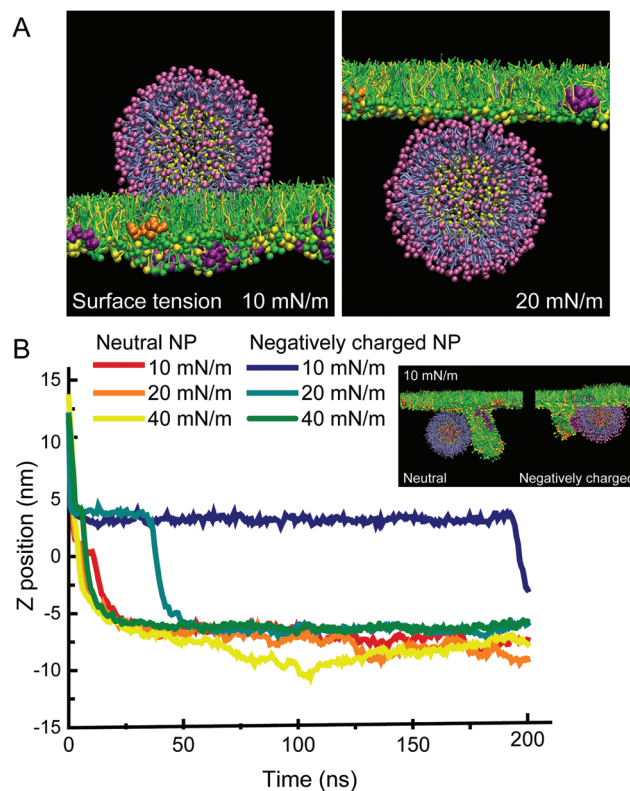


Fig. 7 Effect of the surface tension of the lung surfactant film on the translocation process of the NPs. (A) The final state of the interaction between the lung surfactant and the negatively charged NPs (grafting with chains of 8 monomers with a grafting density of 100%) under different surface tensions. (B) Penetration of NPs across the lung surfactant film under different surface tensions. The dynamic Z position of the neutral and negatively charged NPs (grafting with chains of 10 monomers with a grafting density of 100%) under different surface tensions. The protrusion induced by the penetration of the NPs at a surface tension of 10 mN m^{-1} is especially visualized.

In addition, as the surface tension decreases, the energy cost for repulsing the lipids at the interface to form a pore will linearly increase with the surface pressure expressed as $\gamma_{a/w} - \gamma_{\text{mem}}$ (where $\gamma_{a/w}$ is the air–water surface tension and γ_{mem} is the surface tension of the film). Along this line, due to the high energy cost for repulsing the lipids at the interface at a 10 mN m^{-1} surface tension, the NP likely repulses the lipids to the liquid phase through penetration that induces a protrusion of the film (Fig. 7B). Moreover, the lung surfactant film will collapse with such protrusion when compressed, which is not observable in the absence of the NPs at the same lateral pressure ($\sim 60 \text{ mN m}^{-1}$).⁶¹ This finding is similar to a previous computational observation on the lipid monolayer collapse induced by the hydrophobic NPs.⁶²

The present numerical results can help understand the effect of hydrophilic NPs on the dysfunction of the lung surfactant film. The previous experiments have found that many types of hydrophilic NPs, such as hydroxyapatite NPs, titanium dioxide NPs and charged polymeric NPs, adversely affect the

bio-function of the lung surfactant film.^{16,32,58,63–66} Our simulations suggest that these adverse effects stem from the interactions between the NPs and the individual components of the lung surfactant. The positively charged NPs can adhere to the anionic lipid heads and induce the film curvature, thus slightly increasing the surface tension. The negatively charged NPs are more likely to deplete the surfactant proteins, especially SP-B due to the intrinsic positive charges of the proteins. Although the neutral NPs preferentially penetrate the film with no adsorption or adhesion, they still could deplete the lipids or SP-C molecules, due to their moderate surface polarity. In addition, our simulations suggest that the lung surfactant film under a lower surface tension suffers from the loss of material and collapse after the penetration of NPs more likely, which is worthy of further studying. Nevertheless, it is still difficult to confirm that these adverse effects are responsible for the pulmonary toxicity of the inhaled NPs.

Conclusions

Using the coarse-grained simulations, we explored the interactions between the polymer-grafted Au NPs and the natural lung surfactant film under different grafting conditions (grafting density, polymer length and terminal charge) and different surface tensions. By varying the grafting conditions, we can control the surface properties (polarity or charge) of NPs to regulate the interactions of the NPs with the lipid tails, heads, and proteins, and therefore their translocation processes. We also find that their adverse effects on the lung surfactant result from their affinity with the individual components of the lung surfactant. Particularly, the positively charged NPs will adhere to the lipid heads, and the negatively charged or neutral NPs can possibly deplete the surfactant proteins or lipids through penetration. Therefore, all of them can potentially increase the surface tension. The surface tension of the film will in turn influence the translocation of the NPs and the collapse of the lung surfactant film. In general, NPs with moderate surface polarity and surface charge are the best choice for the inhaled delivery because they can most readily penetrate the lung surfactant film with minimized dysfunction. Although the CGMD simulations can help understand the mechanism of the grafted NP translocation across the lung surfactant film at the mesoscale, there still exist limitations in this research. In comparison with the real biological system, both the temporal and spatial scales of the simulation are much smaller, yielding somehow rough information related to the realistic case. It is worth increasing the size of the modeling system to investigate the size effects if a more powerful computing resource will be available in the future.

Conflicts of interest

There are no conflicts to declare.

Acknowledgements

This work was supported by the NSFC (11832017 and 11572334), the CAS Key Research Program of Frontier Sciences (QYZDB-SW-JSC036), and the CAS Strategic Priority Research Program (XDB22040403) to G. H. The MD simulations were performed on TianHe-1(A) at the National Supercomputing Center in Tianjin.

References

- 1 B. Pelaz, C. Alexiou, R. A. Alvarez-Puebla, F. Alves, A. M. Andrews, S. Ashraf, L. P. Balogh, L. Ballerini, A. Bestetti, C. Brendel, S. Bosi, M. Carril, W. C. Chan, C. Chen, X. Chen, X. Chen, Z. Cheng, D. Cui, J. Du, C. Dullin, A. Escudero, N. Feliu, M. Gao, M. George, Y. Gogotsi, A. Grunweller, Z. Gu, N. J. Halas, N. Hampp, R. K. Hartmann, M. C. Hersam, P. Hunziker, J. Jian, X. Jiang, P. Jungebluth, P. Kadhiresan, K. Kataoka, A. Khademhosseini, J. Kopecek, N. A. Kotov, H. F. Krug, D. S. Lee, C. M. Lehr, K. W. Leong, X. J. Liang, M. L. Lim, L. M. Liz-Marzan, X. Ma, P. Macchiarini, H. Meng, H. Mohwald, P. Mulvaney, A. E. Nel, S. Nie, P. Nordlander, T. Okano, J. Oliveira, T. H. Park, R. M. Penner, M. Prato, V. Puntès, V. M. Rotello, A. Samarakoon, R. E. Schaak, Y. Shen, S. Sjoqvist, A. G. Skirtach, M. G. Soliman, M. M. Stevens, H. W. Sung, B. Z. Tang, R. Tietze, B. N. Udugama, J. S. VanEpps, T. Weil, P. S. Weiss, I. Willner, Y. Wu, L. Yang, Z. Yue, Q. Zhang, Q. Zhang, X. E. Zhang, Y. Zhao, X. Zhou and W. J. Parak, *ACS Nano*, 2017, **11**, 2313–2381.
- 2 R. A. Petros and J. M. DeSimone, *Nat. Rev. Drug Discovery*, 2010, **9**, 615–627.
- 3 J. C. Sung, B. L. Pulliam and D. A. Edwards, *Trends Biotechnol.*, 2007, **25**, 563–570.
- 4 A. Hidalgo, A. Cruz and J. Perez-Gil, *Biochim. Biophys. Acta*, 2017, **1859**, 1740–1748.
- 5 S. Mangal, W. Gao, T. L. Li and Q. Zhou, *Acta Pharmacol. Sin.*, 2017, **38**, 782–797.
- 6 C. A. Ruge, J. Kirch and C. M. Lehr, *Lancet Respir. Med.*, 2013, **1**, 402–413.
- 7 Y. Y. Zuo, R. A. Veldhuizen, A. W. Neumann, N. O. Petersen and F. Possmayer, *Biochim. Biophys. Acta, Biomembr.*, 2008, **1778**, 1947–1977.
- 8 S. Rugonyi, S. C. Biswas and S. B. Hall, *Respir. Physiol. Neurobiol.*, 2008, **163**, 244–255.
- 9 X. Bai, L. Xu, J. Y. Tang, Y. Y. Zuo and G. Hu, *Biophys. J.*, 2019, **117**, 1224–1233.
- 10 J. Perez-Gil, *Biochim. Biophys. Acta*, 2008, **1778**, 1676–1695.
- 11 F. X. McCormack and J. A. Whitsett, *J. Clin. Invest.*, 2002, **109**, 707–712.
- 12 G. Hu, B. Jiao, X. Shi, R. P. Valle, Q. Fan and Y. Y. Zuo, *ACS Nano*, 2013, **7**, 10525–10533.
- 13 Z. Luo, S. Li, Y. Xu, Z. Yan, F. Huang and T. Yue, *Environ. Sci.: Nano*, 2018, **5**, 1921–1932.
- 14 R. K. Harishchandra, M. Saleem and H. J. Galla, *J. R. Soc., Interface*, 2010, **7**, S15–S26.

- 15 M. V. Dwivedi, R. K. Harishchandra, O. Koshkina, M. Maskos and H. J. Galla, *Biophys. J.*, 2014, **106**, 289–298.
- 16 Q. Fan, Y. E. Wang, X. Zhao, J. S. C. Loo and Y. Y. Zuo, *ACS Nano*, 2011, **5**, 6410–6416.
- 17 Y. Yang, L. Xu, S. Dekkers, L. G. Zhang, F. R. Cassee and Y. Y. Zuo, *Environ. Sci. Technol.*, 2018, **52**, 8920–8929.
- 18 E. Guzmán and E. Santini, *Curr. Opin. Colloid Interface Sci.*, 2019, **39**, 24–39.
- 19 R. P. Valle, T. Wu and Y. Y. Zuo, *ACS Nano*, 2015, **9**, 5413–5421.
- 20 Q. L. Hu, X. Bai, G. Q. Hu and Y. Y. Zuo, *ACS Nano*, 2017, **11**, 6832–6842.
- 21 X. Bai, M. Xu, S. J. Liu and G. Q. Hu, *ACS Appl. Mater. Interfaces*, 2018, **10**, 20368–20376.
- 22 A. A. Kapralov, W. H. Feng, A. A. Amoscato, N. Yanamala, K. Balasubramanian, D. E. Winnica, E. R. Kisin, G. P. Kotchey, P. Gou, L. J. Sparvero, P. Ray, R. K. Mallampalli, J. Klein-Seetharaman, B. Fadeel, A. Star, A. A. Shvedova and V. E. Kagan, *ACS Nano*, 2012, **6**, 4147–4156.
- 23 A. J. Thorley, P. Ruenraroengsak, T. E. Potter and T. D. Tetley, *ACS Nano*, 2014, **8**, 11778–11789.
- 24 F. Mousseau, C. Puisney, S. Mornet, R. L. Borgne, A. Vacher, M. Airiau, A. Baeza-Squiban and J. F. Berret, *Nanoscale*, 2017, **9**, 14967–14978.
- 25 S. Mitragotri and J. Lahann, *Nat. Mater.*, 2009, **8**, 15–23.
- 26 C. A. J. Lin, R. A. Sperling, J. K. Li, T. Y. Yang, P. Y. Li, M. Zanella, W. H. Chang and W. G. J. Parak, *Small*, 2008, **4**, 334–341.
- 27 J. Lipka, M. Semmler-Behnke, R. A. Sperling, A. Wenk, S. Takenaka, C. Schleh, T. Kissel, W. J. Parak and W. G. Kreyling, *Biomaterials*, 2010, **31**, 6574–6581.
- 28 J. V. Jokerst, T. Lobovkina, R. N. Zare and S. S. Gambhir, *Nanomedicine*, 2011, **6**, 715–728.
- 29 E. Rytting, J. Nguyen, X. Y. Wang and T. Kissel, *Expert Opin. Drug Delivery*, 2008, **5**, 629–639.
- 30 F. Ungaro, I. d'Angelo, C. Coletta, R. D. D. Bianca, R. Sorrentino, B. Perfetto, M. A. Tufano, A. Miro, M. I. La Rotonda and F. Quaglia, *J. Controlled Release*, 2012, **157**, 149–159.
- 31 M. Beck-Broichsitter, C. Ruppert, T. Schmehl, A. Günther and W. Seeger, *Acta Biomater.*, 2014, **10**, 4678–4684.
- 32 M. Beck-Broichsitter, C. Ruppert, T. Schmehl, A. Guenther, T. Betz, U. Bakowsky, W. Seeger, T. Kissel and T. Gessler, *Nanomedicine*, 2011, **7**, 341–350.
- 33 M. Beck-Broichsitter, C. Ruppert, T. Schmehl, A. Gunther and W. Seeger, *Biochim. Biophys. Acta, Biomembr.*, 2014, **1838**, 474–481.
- 34 K. Yang and Y. Q. Ma, *Nat. Nanotechnol.*, 2010, **5**, 579–583.
- 35 Y. Xu, Z. Luo, S. X. Li, W. G. Li, X. R. Zhang, Y. Y. Zuo, F. Huang and T. T. Yue, *Nanoscale*, 2017, **9**, 10193–10204.
- 36 S. Baoukina and D. P. Tieleman, *Biochim. Biophys. Acta, Biomembr.*, 2016, **1858**, 2431–2440.
- 37 H. M. Ding and Y. Q. Ma, *Small*, 2015, **11**, 1055–1071.
- 38 L. Martinez, R. Andrade, E. G. Birgin and J. M. Martinez, *J. Comput. Chem.*, 2009, **30**, 2157–2164.
- 39 J. Q. Lin, H. W. Zhang, Z. Chen and Y. G. Zheng, *ACS Nano*, 2010, **4**, 5421–5429.
- 40 S. J. Marrink, H. J. Risselada, S. Yefimov, D. P. Tieleman and A. H. de Vries, *J. Phys. Chem. B*, 2007, **111**, 7812–7824.
- 41 F. C. Bernstein, T. F. Koetzle, G. J. Williams, E. F. Meyer Jr., M. D. Brice, J. R. Rodgers, O. Kennard, T. Shimanouchi and M. Tasumi, *J. Mol. Biol.*, 1977, **112**, 535–542.
- 42 M. Sarker, A. J. Waring, F. J. Walther, K. M. W. Keough and V. Booth, *Biochemistry*, 2007, **46**, 11047–11056.
- 43 F. Baumgart, O. L. Ospina, I. Mingarro, I. Rodriguez-Crespo and J. Perez-Gil, *Biophys. J.*, 2010, **99**, 3234–3243.
- 44 F. J. Walther, A. J. Waring, M. A. Sherman, J. A. Zasadzinski and L. M. Gordon, *Neonatology*, 2007, **91**, 303–310.
- 45 D. Van der Spoel, E. Lindahl, B. Hess, G. Groenhof, A. E. Mark and H. J. C. Berendsen, *J. Comput. Chem.*, 2005, **26**, 1701–1718.
- 46 S. Zhang, H. Gao and G. Bao, *ACS Nano*, 2015, **9**, 8655–8671.
- 47 A. Verma and F. Stellacci, *Small*, 2010, **6**, 12–21.
- 48 A. H. Bahrami, M. Raatz, J. Agudo-Canalejo, R. Michel, E. M. Curtis, C. K. Hall, M. Gradzielski, R. Lipowsky and T. R. Weikl, *Adv. Colloid Interface Sci.*, 2014, **208**, 214–224.
- 49 Y. Tu, M. Lv, P. Xiu, T. Huynh, M. Zhang, M. Castelli, Z. Liu, Q. Huang, C. Fan, H. Fang and R. Zhou, *Nat. Nanotechnol.*, 2013, **8**, 594–601.
- 50 R. H. Notter, J. N. Finkelstein and R. D. Taubold, *Chem. Phys. Lipids*, 1983, **33**, 67–80.
- 51 Y. Li and N. Gu, *J. Phys. Chem. B*, 2010, **114**, 2749–2754.
- 52 Y. Li, X. Chen and N. Gu, *J. Phys. Chem. B*, 2008, **112**, 16647–16653.
- 53 Y. Li, M. Kroger and W. K. Liu, *Biomaterials*, 2014, **35**, 8467–8478.
- 54 X. Lin, T. Bai, Y. Y. Zuo and N. Gu, *Nanoscale*, 2014, **6**, 2759–2767.
- 55 C.-c. Chiu, W. Shinoda, R. H. DeVane and S. O. Nielsen, *Soft Matter*, 2012, **8**, 9610.
- 56 E. Guzman, M. Ferrari, E. Santini, L. Liggieri and F. Ravera, *Colloids Surf., B*, 2015, **136**, 971–980.
- 57 C. Alonso, T. Alig, J. Yoon, F. Bringezu, H. Warriner and J. A. Zasadzinski, *Biophys. J.*, 2004, **87**, 4188–4202.
- 58 M. Beck-Broichsitter, *Langmuir*, 2016, **32**, 10422–10429.
- 59 R. W. Walters, R. R. Jenq and S. B. Hall, *Biophys. J.*, 2000, **78**, 257–266.
- 60 C. Casals and O. Canadas, *Biochim. Biophys. Acta*, 2012, **1818**, 2550–2562.
- 61 S. Baoukina, L. Monticelli, H. J. Risselada, S. J. Marrink and D. P. Tieleman, *Proc. Natl. Acad. Sci. U. S. A.*, 2008, **105**, 10803–10808.
- 62 J. Barnoud, L. Urbini and L. Monticelli, *J. R. Soc., Interface*, 2015, **12**, 20140931.
- 63 D. Q. Arick, Y. H. Choi, H. C. Kim and Y. Y. Won, *Adv. Colloid Interface Sci.*, 2015, **225**, 218–228.
- 64 E. Guzman, E. Santini, M. Ferrari, L. Liggieri and F. Ravera, *Langmuir*, 2017, **33**, 10715–10725.
- 65 C. Peetla and V. Labhasetwar, *Mol. Pharmaceutics*, 2008, **5**, 418–429.
- 66 S. Behyan, O. Borozenko, A. Khan, M. Faral, A. Badia and C. DeWolf, *Environ. Sci.: Nano*, 2018, **5**, 1218–1230.